

DST-Net: A Dual-Stream Transformer with Illumination-Independent Feature Guidance and Multi-Scale Spatial Convolution for Low-Light Image Enhancement

Yicui Shi^a, Yuhan Chen^a, Xiangfei Huang^a, Zhenguo Wang^b, Wenxuan Yu^a and Ying Fang^a

^aCollege of Mechanical and Vehicle Engineering, Chongqing University, Chongqing, 400044, China

^bShanghai Zhenhua Heavy Industries Co.,Ltd., Shanghai, 200125, China

ARTICLE INFO

Keywords:

Low-light image enhancement
Transformer
3D Convolution

ABSTRACT

Low-light image enhancement aims to restore the visibility of images captured by visual sensors in dim environments by addressing their inherent signal degradations, such as luminance attenuation and structural corruption. Although numerous algorithms attempt to improve image quality, existing methods often cause a severe loss of intrinsic signal priors. They struggle to achieve substantial brightness improvements while maintaining color fidelity, preserving geometric structures, and recovering high-frequency fine textures. To overcome these challenges, we propose a Dual-Stream Transformer Network (DST-Net) based on illumination-agnostic signal prior guidance and multi-scale spatial convolutions. First, to address the loss of critical signal features under low-light conditions, we design a feature extraction module. This module integrates Difference of Gaussians (DoG), LAB color space transformations, and VGG-16 for texture extraction, utilizing decoupled illumination-agnostic features as signal priors to continuously guide the enhancement process. Second, we construct a dual-stream interaction architecture. By employing a cross-modal attention mechanism, the network leverages the extracted priors to dynamically rectify the deteriorated signal representation of the enhanced image, ultimately achieving iterative enhancement through differentiable curve estimation. Furthermore, to overcome the inability of existing methods to preserve fine structures and textures, we propose a Multi-Scale Spatial Fusion Block (MSFB) featuring pseudo-3D and 3D gradient operator convolutions. This module integrates explicit gradient operators to recover high-frequency edges while capturing inter-channel spatial correlations via multi-scale spatial convolutions. Extensive evaluations and ablation studies demonstrate that DST-Net achieves superior performance in subjective visual quality and objective metrics. Specifically, our method achieves a PSNR of 25.64 dB on the LOL dataset. Subsequent validation on the LSRW dataset further confirms its robust cross-scene generalization.

1. Introduction

Rapid advancements in visual sensor technology have driven the widespread deployment of image acquisition devices in fields like autonomous driving, video surveillance, and smartphone photography. Although the performance of modern sensor hardware continues to improve, acquiring clear visual signals remains a severe challenge in adverse lighting environments like nighttime, backlighting, or extreme low illumination [1–3]. Constrained by limited exposure times and the physical properties of photosensitive elements, images captured in dim environments typically suffer from severe signal degradations, including insufficient luminance, compressed dynamic ranges, and heavy noise artifacts [4]. Such signal degradations cause the loss of critical object information, compromising human subjective perception and hindering computer vision algorithms reliant on clear feature inputs [5, 6].

Therefore, developing efficient low-light image enhancement algorithms to effectively restore underlying signal structures and high-frequency texture details while increasing luminance holds substantial theoretical and practical value for improving the all-weather adaptability of visual systems [7]. Convolutional Neural Network (CNN) and Transformer-based algorithms have gradually replaced traditional methods, dominating the field of low-light image enhancement [4, 7, 8]. Leveraging strong local feature extraction capabilities, CNN-based methods effectively learn

*Corresponding author

✉ yicuishicqu.edu.cn (Y. Shi); 20240701028@stu.cqu.edu.cn (Y. Chen); hx0213@stu.cqu.edu.cn (X. Huang); wangzhenguo_ssz@zpmc.com (Z. Wang); wenxuanyu@cqu.edu.cn (W. Yu); yingfang@stu.cqu.edu.cn (Y. Fang); liguofa@cqu.edu.cn (Y. Fang)

ORCID(s):

low-light to normal-light mappings or estimate physical illumination parameters [9]. Meanwhile, recent Transformer architectures employ self-attention mechanisms to capture long-range dependencies, further improving the global consistency of the enhanced results [10–12].

Despite the significant progress of data-driven methods, most existing approaches focus on pixel-level luminance enhancement, often overlooking the preservation of structural and textural details inherent in illumination-Independent signals [9]. Consequently, these models struggle to achieve substantial luminance improvements while maintaining color fidelity, geometric integrity, and fine texture details. More importantly, existing algorithms often cause a severe loss of critical signal features during complex non-linear enhancement processes. The enhanced images frequently exhibit blurred edges or details obscured by noise, failing to meet the demands of high-precision downstream vision tasks [13, 14].

While deep learning-based methods have advanced significantly, mainstream iterative low-light enhancement algorithms such as Zero-DCE [15], and Zero-DCE++ [16] still struggle with signal feature preservation. These approaches typically rely on pixel-level curve estimation or weight mapping to iteratively increase image luminance. However, such strategies focusing solely on pixel intensity adjustments often neglect intrinsic semantic information and structural features [7, 17]. Due to the lack of explicit constraints and protection for high-level features during multi-stage iterative enhancement, high-frequency texture details and edge structures in the degraded signals often suffer irreversible degradation alongside non-linear luminance stretching. In other words, despite effectively illuminating dark regions, these methods sacrifice critical image features and ultimately fail to meet the demands of high-quality visual perception [18, 19].

Incorporating feature-level enhancement strategies is crucial for preserving the authenticity of image content in restoration tasks [20, 21]. Prior-guided signal enhancement strengthens the representational capacity of networks while effectively retaining critical information during complex transformations [19, 22]. Inspired by this, we propose an enhancement scheme guided by illumination-independent signal features. Unlike directly manipulating RGB pixels, our DST-Net focuses on extracting and preserving intrinsic illumination-independent signal priors from low-light images, including textures, geometric structures, and color components. These stable feature maps serve as signal prior information to continuously guide the low-light image enhancement process. Through this mechanism, the network leverages the extracted feature maps to perform spatially adaptive adjustments across different regions of the low-light image by suppressing noise in smooth areas and reinforcing high-frequency details in texture-rich zones. This dual-stream interaction design ensures that we meticulously restore fine texture details and structural integrity while achieving global luminance enhancement, thereby delivering superior visual quality.

To overcome the aforementioned challenges, particularly the severe loss of feature information caused by existing iterative methods confined to pixel-level mappings, we propose a Dual-Stream Transformer Network (DST-Net) based on illumination-independent signal prior enhancement and multi-scale spatial fusion convolutions. Moving beyond the limitations of traditional end-to-end mappings, our DST-Net primarily consists of three core components: First, to overcome signal feature degradation under low-light conditions, we design an illumination-independent feature extraction module. This module integrates Difference of Gaussians (DoG), LAB color space transformations, and VGG-16 texture features to construct intrinsic representations decoupled from luminance, thereby providing continuous and stable signal prior guidance throughout the enhancement process. Second, we introduce an improved dual-stream Transformer interaction architecture. By employing a cross-modal attention mechanism, our network leverages the extracted illumination-independent features to dynamically rectify the deteriorated signal representation of the enhanced image, ultimately achieving high-fidelity iterative enhancement via differentiable curve estimation.

Furthermore, to overcome the inability of existing Convolutional Neural Networks (CNNs) to capture inter-channel spatial correlations and prevent the resulting blurring of high-frequency fine textures, we develop a Multi-Scale Spatial Fusion Block (MSFB) featuring pseudo-3D convolutions. This module integrates explicit gradient operators such as Sobel and Laplacian to recover high-frequency edge details while exploiting deep spatial correlations along the channel dimension via multi-scale channel convolutions, thereby significantly enhancing the capability of our model to preserve geometric structures under extremely low signal-to-noise ratios.

The main contributions of this paper are summarized as follows:

- We propose a Multi-Scale Spatial Fusion Block (MSFB) featuring pseudo-3D convolutions. By integrating multi-scale voxel spatial convolutions and explicit 3D gradient operators such as Sobel and Laplacian, this module effectively exploits inter-channel spatial correlations, significantly enhancing the capability of the network to capture geometric structures and high-frequency fine textures in low signal-to-noise ratio environments.

- We leverage decoupled low-light color, structure, and texture feature maps as signal priors. By employing a cross-modal attention mechanism and iterative differentiable curve estimation, we dynamically rectify the deteriorated signal representation during the enhancement process, thereby ensuring exceptional image fidelity while substantially increasing luminance.
- Extensive ablation studies and comparative evaluations on benchmark datasets such as LOL, LSRW-N, and LSRW-H demonstrate that our proposed method achieves outstanding performance in subjective visual quality and objective metrics, exhibiting robust cross-scene generalization capabilities.

2. Related Work

2.1. Low-Light Enhancement

2.1.1. Traditional Methods

Early approaches to low-light image enhancement primarily relied on Histogram Equalization (HE) and Retinex theory. HE improves global contrast by expanding the dynamic range of images. To mitigate the loss of local details caused by global HE, Pizer et al. [23] proposed Contrast Limited Adaptive Histogram Equalization (CLAHE) to suppress noise over-amplification by restricting the height of local histograms. Furthermore, Gamma Correction [24] serves as a widely adopted non-linear transformation technique to adjust the luminance distribution of images. Beyond statistical approaches, algorithms based on Retinex theory assume that observed images can be decomposed into illumination and reflectance components. Following the initial introduction of Retinex theory by Land [25], Jobson et al. [26] developed Single-Scale Retinex (SSR) and Multi-Scale Retinex (MSR) algorithms to estimate the illumination component via Gaussian filtering. Building on this foundation, Guo et al. [27] proposed the LIME method to improve enhancement quality by imposing structural priors on the illumination map.

2.1.2. Deep-Learning Methods

While traditional physics-based models such as LIME have achieved notable success via illumination map estimation, data-driven approaches have gradually become the mainstream paradigm owing to the powerful feature representation capabilities of deep neural networks. Early deep learning methods primarily focused on constructing algorithm unrolling networks based on Retinex theory to balance physical interpretability with the robust fitting capacity of deep models. For instance, Liu et al. [28] utilized neural architecture search to construct RUAS, an unrolling architecture with cooperative priors. Wu et al. [29] designed URetinex-Net by unfolding the decomposition process into physically constrained deep modules, while Zheng et al. [30] introduced an adaptive unrolling total variation network for noise smoothing. Furthermore, Fu et al. [31] explored learning simple yet effective enhancers from paired low-light data.

To eliminate the dependency on paired data and improve inference efficiency, unsupervised learning and iterative curve estimation methods have gained prominence. Jiang et al. [32] pioneered EnlightenGAN by utilizing unpaired generative adversarial networks for unsupervised enhancement. Subsequently, Guo et al. [15] introduced Zero-DCE, which reformulates the enhancement task as a pixel-level high-order curve estimation problem, a framework later refined by Li et al. [16] in Zero-DCE++. Seeking faster convergence and superior performance, Ma et al. [33] developed SCI, leveraging a weight-sharing mechanism for ultra-fast iteration. Pan et al. [34] introduced Chebyshev polynomial approximation to determine optimal enhancement curves. Meanwhile, Liu et al. [35] explored iterative mechanisms for combined enhancement and fusion via EFINet.

Recently, several advanced algorithms have emerged, achieving breakthroughs in both efficiency and robustness. Chen et al. introduced FMR-Net [36] and FRR-Net [37] to significantly optimize network performance through multi-scale residuals and re-parameterization techniques. To handle intractable noise and artifacts, Zhang et al. [38] proposed a noise autoregressive learning paradigm that enables joint denoising and enhancement without task-specific data. Similarly, Shi et al. [39] developed ZERO-IG for zero-shot illumination-guided joint denoising. Furthermore, Chen et al. [40] designed a lightweight real-time enhancement network, delivering superior visual quality while maintaining low computational complexity.

2.2. Multi-scale Feature Extraction Block

Extracting multi-scale contextual information is a pivotal strategy for addressing scale variations and detail restoration in image enhancement. To overcome the restricted receptive fields of single-scale convolutions, various hierarchical architectures aim to capture diverse structural information. For instance, Li et al. [41] proposed the

Multi-Scale Residual Block (MSRB), utilizing parallel convolutional layers with different kernel sizes to detect multi-frequency image features while promoting efficient information flow through local residual connections. Inspired by these designs, MIRNet [42] integrates multi-scale residual structures into multi-resolution streams to enable effective cross-scale feature interaction. Similarly, FMR-Net [36] incorporates multi-scale residual attention, while Cho et al. [43] achieve coarse-to-fine feature refinement via multi-scale pyramid reconstruction.

Attention-based mechanisms are widely employed to adaptively calibrate feature responses during fusion and recalibration. For instance, Dai et al. [44] introduced Attentional Feature Fusion (AFF) to dynamically calculate fusion weights by integrating local and global contextual attention. Similarly, Hu et al. [45] and Woo et al. [46] respectively introduced SE-Net and CBAM to recalibrate feature responses along channel or spatial dimensions to enhance network sensitivity to critical information. Additionally, Liu et al. [47] developed FFA-Net to explore the potential of pixel-level weighting for addressing non-uniform degradation via a Feature Attention (FA) module. To address spatial correlations across feature channels, we explore a Pseudo-3D architecture. This design exploits voxel-level spatial correlations similar to 3D convolutions. It avoids the redundancy inherent in full 3D operations and maintains the computational efficiency of 2D convolutions.

2.3. Dual-Stream Feature Guidance

Single-stream networks often struggle to balance global luminance adjustment and local detail restoration under complex noise and degradation. Consequently, dual-stream architectures utilizing feature enhancement have emerged as a prevalent paradigm. Wei et al. [48] pioneered RetinexNet based on Retinex theory. Zhang et al. [49] refined this framework in KinD by decoupling illumination adjustment and reflectance denoising modules. Utilizing auxiliary feature maps as prior information guides the enhancement process alongside physical component decoupling. Ma et al. [50] proposed a Structure-Map-Guided (SMG) strategy. Xu et al. [51] designed SNR-Net to construct spatially-varying feature guidance via Signal-to-Noise Ratio (SNR) maps.

Transformer architectures have facilitated increasingly flexible and efficient cross-modal feature guidance. Cui et al. [52] proposed the Illumination-Adaptive Transformer (IAT). Cai et al. [53] integrated illumination priors into the self-attention mechanism within Retinexformer. Xu et al. [20] introduced UPT-Flow, employing unbalanced point maps to guide normalizing flow models and rectify non-uniform RGB distributions. To address these limitations, we utilize extracted illumination-Independent texture, structure, and color features as Key and Value to continuously guide the learning of original image features serving as the Query.

3. Proposed Method

3.1. Overall Pipeline

Figure 1 illustrates the overall architecture of DST-Net. We develop an enhancement framework based on dual-stream interaction. For a given low-light input image $I \in \mathbb{R}^{H \times W \times 3}$, the pipeline commences with a specialized illumination-independent feature extraction module. This module integrates structural information from the Difference of Gaussians (DoG), chromaticity components from the LAB color space, and texture features extracted via VGG-16. This design decouples physical features insensitive to illumination variations from the low-light input and subsequently injects these features into the auxiliary stream to serve as signal prior guidance. The extracted structural, chromaticity, and texture features undergo continuous information exchange and deep enhancement with the low-light image via a cross-modal dual-stream Transformer architecture.

The feature stream leverages its preserved structural information to dynamically rectify noise-corrupted signal distributions within the image stream. We integrate a Multi-Scale Spatial Fusion Block (MSFB) during this encoding process to capture spatial correlations across channels more precisely. This module utilizes Pseudo-3D convolutions coupled with explicit Pseudo-3D gradient operators such as Sobel and Laplacian to facilitate the deep extraction of high-frequency details and edge information.

For the final image reconstruction stage, we adopt a strategy that combines feature fusion with residual compensation. The network concatenates refined features from the dual-stream Transformer with initial shallow features and the original low light image along the channel dimension to preserve comprehensive contextual information. Subsequently, we convolve the fused features and add them to the residual term generated by the iterative enhancement module. This ensures that the final enhanced image integrates fine-grained details captured by the Transformer with global signal amplitude adjustments obtained through iterative curve estimation. We design this residual connection to maximize geometric and chromatic fidelity while effectively enhancing brightness.

representation \mathcal{F}_{tex} :

$$\mathcal{F}_{tex} = P_{vgg}(\mathcal{R}(I_{in})) \quad (3)$$

where P_{vgg} denotes the feature projection transformation of VGG-16, while $\mathcal{R}(\cdot)$ signifies necessary resizing and preprocessing operations.

Finally, we perform multi-scale fusion of the complementary structural, chromatic, and textural features along the channel dimension to generate the comprehensive illumination-independent guidance feature \mathcal{F}_{inv} :

$$\mathcal{F}_{inv} = \text{Cat}(\mathcal{F}_{dog}, \mathcal{F}_{color}, \mathcal{F}_{tex}) \quad (4)$$

\mathcal{F}_{inv} incorporates low-level geometric edges and physical colors alongside high-level semantic textures. This fusion provides comprehensive prior guidance for subsequent dual-stream Transformer interaction.

3.2.2. Transformer Feature Extraction Block

As shown in Fig. 2, Let X_I^l and X_F^l denote the image and feature stream features at the l -th layer. We project the low light image stream features as the Query within the cross-attention module while utilizing the features as the Key and Value to integrate pertinent texture details. We compute the matrices Q , K , and V as follows:

$$Q = X_I^l W_Q, \quad K = X_F^l W_K, \quad V = X_F^l W_V \quad (5)$$

The variables W_Q , W_K , and W_V denote learnable linear projection matrices. We calculate the cross-modal attention map via a scaled dot-product based on these matrices. This operation fuses guidance information to yield the intermediate feature \tilde{X}_I^l :

$$\tilde{X}_I^l = X_I^l + \text{Softmax}\left(\frac{QK^T}{\sqrt{d_k}}\right)V \quad (6)$$

The variable d_k denotes the scaling factor.

Different channels in the feature maps contribute unequally to the restoration task following cross-modal interaction. We introduce a Lightweight Channel Attention (LCA) module to adaptively recalibrate channel dependencies. LCA utilizes both Global Average Pooling (AvgPool) and Global Max Pooling (MaxPool) to aggregate spatial contextual information. This aggregation generates channel descriptors:

$$F_{avg} = \text{AvgPool}(\tilde{X}_I^l), \quad F_{max} = \text{MaxPool}(\tilde{X}_I^l) \quad (7)$$

Subsequently, we feed these two descriptors into a shared Multi-Layer Perceptron (MLP) to capture inter-channel non-linear relationships. This MLP consists of two 1×1 convolutional layers separated by a ReLU activation function. We calculate the final channel attention weight M_c as follows:

$$M_c(\tilde{X}_I^l) = \sigma(\text{MLP}(F_{avg}) + \text{MLP}(F_{max})) \quad (8)$$

where σ denotes the Sigmoid activation function. We obtain the image stream output X_I^{l+1} at the $(l+1)$ -th layer by applying the learned channel weights to the normalized intermediate features. This operation recalibrates the response of each channel to highlight informative features while suppressing noise:

$$X_I^{l+1} = \text{LN}(\tilde{X}_I^l) \odot M_c(\tilde{X}_I^l) \quad (9)$$

This dual interaction-recalibration mechanism enables the network to leverage external illumination-independent features for macro-guidance and execute micro-level feature screening through internal channel attention. This design maximizes noise suppression while preserving intricate texture details throughout the enhancement process.

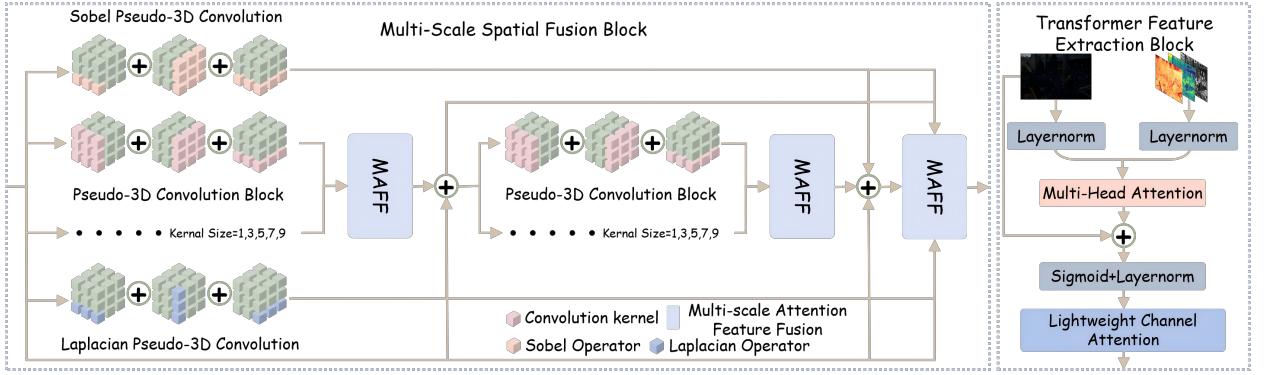


Figure 2: Overall Network Architecture of TFEB and MSFB.

3.3. Multi-Scale Spatial Fusion Block

Traditional 2D convolutions often neglect spatial correlations across feature channels, whereas standard 3D convolutions incur prohibitive computational costs. We propose the Multi-Scale Spatial Fusion Block (MSFB) to capture voxel-level spatial-channel dependencies and reinforce edge details while maintaining computational efficiency. As shown in Fig. 2, MSFB comprises three parallel branches: an explicit gradient injection branch, a multi-scale Pseudo-3D convolution branch, and a hierarchical attention fusion mechanism.

To heighten sensitivity to high-frequency details, we embed gradient priors directly into the feature extraction process. We design Pseudo-3D Laplacian and Sobel operators to capture isotropic texture details and anisotropic edge gradients. For an input feature $X \in \mathbb{R}^{C \times H \times W}$, the gradient branch operates as follows:

$$\mathcal{F}_{Lap} = \text{GELU} \left(\sum_{d \in \{x,y,z\}} |X \otimes K_{Lap}^d| \right), \quad \mathcal{F}_{Sob} = \text{GELU} \left(\sum_{d \in \{x,y,z\}} |X \otimes K_{Sob}^d| \right) \quad (10)$$

Here \otimes denotes 3D convolution. K_{Lap}^d and K_{Sob}^d represent discrete differential kernels along the width, height, and channel directions respectively. This decomposed computation scheme effectively reduces the total number of parameters. The approach also prevents over-smoothing during the denoising process.

We design a multi-scale Pseudo-3D (P3D) residual block to capture spatial-channel correlations across diverse receptive fields. The P3D block differs from standard convolutions by decomposing a $k \times k \times k$ 3D convolution into three orthogonal plane convolutions. These components include the channel-height convolution C_{ch} , the channel-width convolution C_{cw} , and the spatial height-width convolution C_{hw} . We also integrate an orthogonal decomposition convolution for the origin projection O . We calculate the output feature M_i for the i -th scale branch as follows:

$$M_i = \text{ReLU} \left(\text{Conv2D} \left(\sum_{p \in \{ch, cw, hw, O\}} \text{ReLU}(\text{Conv}_{3D}^p(X)) \right) + X \right) \quad (11)$$

We propose the Multi-scale Attention Feature Fusion (MAFF) module to integrate features across various scales effectively. This architecture is designated as MAFF. We describe the internal processing flow as follows:

$$\begin{aligned} \mathcal{F}_{att} &= \text{Attn}_{S+C}(\text{ReLU}(\Phi_{local}(\mathcal{F}_{in}) + \Phi_{global}(\mathcal{F}_{in}))) \\ \omega_i &= \text{Softmax}(\Psi([\sigma(\text{Rep}_i(\mathcal{F}_{att})) \otimes f_i]_{i=1}^5)) \\ \mathcal{F}_{out} &= \text{Conv} \left(\sum_{i=1}^5 \omega_i \cdot f_i \right) \end{aligned} \quad (12)$$

where Attn_{S+C} achieves fine-grained feature refinement through the sequential integration of spatial and channel attention. Specialized representations are generated for each branch by Rep_i to extract salient features. Ψ maps these

enhanced features to a decision space to calculate normalized weights ω_i . These weights ensure the dynamic and complementary integration of input branches during the fusion process.

We adopt a hierarchical strategy to aggregate features $\mathcal{M}_k = \{M_k\}_{k \in \{1,3,5,7,9\}}$ progressively within the MSFB module. We define this process as follows:

$$\begin{aligned} H_1 &= \text{MAFF}_1(\mathcal{M}_k(X)) + \mathcal{F}_{Lap} + X \\ H_2 &= \text{MAFF}_2(\mathcal{M}_k(H_1)) + \mathcal{F}_{Sob} + X + H_1 \end{aligned} \quad (13)$$

The variables H_1 and H_2 represent the fused features of the first and second stages, respectively. The module integrates all computational paths to generate the final feature Y_{MSFB} in the concluding step:

$$Y_{MSFB} = \text{MAFF}_3(H_2, H_1, \mathcal{F}_{Lap}, \mathcal{F}_{Sob}, X) + \text{GELU}(\text{Conv}_{res}(X)) \quad (14)$$

3.4. Deep Feature-Guided Iterative Curve Enhancement

While the dual-stream Transformer and MSFB modules effectively perform feature extraction and detail restoration, directly regressing pixel values via convolutional networks often induces color bias or uneven luminance. We propose a Deep Feature-Guided Iterative Curve Estimation strategy to achieve natural illumination enhancement while maintaining signal processing stability. This strategy leverages deep semantic features extracted by the dual-stream Transformer to generate high-order curve parameters, enabling precise and adaptive adjustments for complex lighting scenarios. Parameter map estimation serves as the core of the curve enhancement process.

At the decoder output, we fuse the image stream feature Y_{up}^3 and feature stream feature X_{up}^3 to generate the enhanced feature map F_{boost} . To further incorporate multi-scale context, we feed F_{boost} into an additional MSFB module for feature refinement:

$$F_{boost} = \mathcal{M}_{boost}(X_{up}^3 + Y_{up}^3) \quad (15)$$

Subsequently, we partition F_{boost} along the channel dimension into K groups of parameter maps $A = \{A_1, A_2, \dots, A_K\}$. The variable K denotes the number of iterations. We set $K = 4$ in this study. A_n represents the pixel-level adjustment coefficient for the n -th iteration. We introduce a specific pixel-level high-order curve to adjust the dynamic range of the image progressively. This curve is differentiable and monotonic within the interval $(0, 1)$. This mathematical property effectively avoids overexposure and artifacts. We define the n -th level enhancement result $LE_n(x)$ as follows given the input image I_{in} and the parameter map A_n :

$$LE_n(x) = LE_{n-1}(x) + A_n(x) \times (LE_{n-1}(x) - LE_{n-1}(x)^2) \quad (16)$$

where x denotes pixel coordinates and $LE_0(x) = I_{in}(x)$ defines the initial state. The quadratic term $LE_{n-1}(x)^2$ imposes a nonlinear constraint that enables the enhancement process to adaptively stretch dark regions and suppress highlights. After K iterations, we obtain the global illumination-enhanced image $I_{curve} = LE_K(x)$. This iterative strategy simulates progressive light-filling to ensure a natural transition of overall brightness.

While curve estimation effectively recovers global illumination, it may neglect certain high-frequency textures. To address this limitation, we treat the fine feature F_{fine} from the Transformer as a texture residual term and superimpose it on the enhanced result I_{curve} :

$$F_{fine} = \mathcal{M}_{end}(\text{Cat}(X_{out}, Y_{out}, I_{in}, I_{feat})) \quad (17)$$

$$I_{final} = \sigma(\text{Conv}_{out}(F_{fine} + I_{curve})) \quad (18)$$

3.5. Loss Functions

We design a multi-constraint objective function to restore brightness while accurately preserving geometric structures and color fidelity. This objective function includes pixel reconstruction, perceptual structural similarity, noise-resistant spatial consistency, and color supervision.

We adopt the L_1 loss as the fundamental constraint to ensure high consistency between the enhanced image I_{est} and the reference normal-light image I_{gt} regarding color and luminance. The L_1 loss exhibits lower sensitivity to outliers

compared with the L_2 loss. This property helps prevent gradient explosion during the training process. The use of L_1 loss also facilitates the generation of sharper edges:

$$\mathcal{L}_1 = \frac{1}{N} \sum_{p \in \Omega} |I_{est}(p) - I_{gt}(p)| \quad (19)$$

where I_{gt} represents the reference image. The variable N denotes the total number of pixels.

We utilize the Structural Similarity (SSIM) loss to constrain the luminance, contrast, and structural components of the image. This constraint addresses the inherent sensitivity of the human visual system to structural information. Our approach prevents the degradation of high-frequency textures during the illumination enhancement process. We define the SSIM loss as follows:

$$\mathcal{L}_{ssim} = 1 - \frac{1}{M} \sum_{j=1}^M \text{SSIM}(I_{est}^{(j)}, I_{gt}^{(j)}) \quad (20)$$

where M denotes the number of sliding windows.

We incorporate two physical prior constraints during training to compensate for the limitations of single supervised learning. These constraints also mitigate noise amplification and under-exposure issues common in low signal-to-noise ratio environments. We introduce an exposure control loss to regulate image exposure levels explicitly. This loss measures the distance between the average intensity value μ_k of local region K in the enhanced image and the target exposure level E . We empirically set the value of E to 0.6:

$$\mathcal{L}_{exp} = \frac{1}{K} \sum_{k=1}^K |\mu_k(I_{est}) - E| \quad (21)$$

However, stretching contrast during low-light enhancement frequently amplifies latent noise. To suppress such high-frequency artifacts, we introduce Total Variation (TV) loss as a smoothing regularization term. \mathcal{L}_{tv} minimizes image gradient magnitudes to promote the generation of piecewise-smooth results, defined as follows:

$$\mathcal{L}_{tv} = \frac{1}{CHW} \sum_{c,h,w} \left((\nabla_x I_{est}^{c,h,w})^2 + (\nabla_y I_{est}^{c,h,w})^2 \right) \quad (22)$$

The variables ∇_x and ∇_y represent the horizontal and vertical gradient differences, respectively. This loss term maintains the sharpness of primary edges during noise removal. Such a mechanism establishes a closed loop of extraction and constraint with the explicit gradient injection design in our MSFB module.

Drastic illumination enhancement often leads to severe color shifts and oversaturation in low-light image restoration tasks. We introduce a color fidelity loss \mathcal{L}_{hsv} based on the HSV color space to supervise color information. This color space comprises Hue, Saturation, and Value components. We apply a minimum circular distance to Hue (H) to avoid mathematical truncation between red and purple. We also employ an L_1 constraint for Saturation (S):

$$\mathcal{L}_{hsv} = \frac{1}{N} \sum_{p \in \Omega} \left[\lambda_{hue} \cdot \min(|H_{ref}^p - H_{est}^p|, 2\pi - |H_{ref}^p - H_{est}^p|) + \lambda_{sat} \cdot |S_{ref}^p - S_{est}^p| \right] \quad (23)$$

where λ_{hue} and λ_{sat} are the trade-off weights for the hue and saturation loss terms, respectively, both of which are set to 1 in our experiments. H_{ref}^p and H_{est}^p denote the hue values of the reference (ground truth) and the estimated (enhanced) images at pixel p , while S_{ref}^p and S_{est}^p represent their corresponding saturation values.

We define the final loss function of DST-Net as a weighted combination of the four components discussed previously. The formula is expressed as follows:

$$\mathcal{L}_{total} = \mathcal{L}_1 + w_1 \mathcal{L}_{ssim} + w_2 \mathcal{L}_{exp} + w_3 \mathcal{L}_{tv} + \mathcal{L}_{hsv} \quad (24)$$

4. Experiments

We evaluate DST-Net using the LOL [48], LSRW-HUAWEI, and LSRW-NIKON [54] datasets. The LOL dataset represents the inaugural benchmark providing authentic paired images for low-light enhancement and contains 500



Figure 3: Qualitative comparison of DST-Net with other state-of-the-art algorithms on the LOL dataset.

pairs of synthetic and captured low-light/normal-light samples. We further utilize the Large-Scale Real-World (LSRW) dataset to assess model adaptability across broader scenarios and diverse acquisition hardware. This benchmark comprises two subsets of paired images captured with HUAWEI P40 Pro and NIKON D7500 devices, respectively.

We implement the DST-Net architecture using the PyTorch 2.1.1 framework. We conduct all training and inference sessions on a computational platform equipped with an NVIDIA vGPU with 32GB of memory. For network optimization, we utilize the Adam optimizer with an initial learning rate of 0.005 and a batch size of 9. We employ a step learning rate decay strategy to prevent training oscillations and ensure convergence, reducing the learning rate by a factor of 0.5 every 50 epochs. We partition all datasets into training and testing sets according to a 9:1 ratio. To maintain input consistency and accommodate multi-scale convolutions, we crop all training image pairs to 192×192 pixel patches using a center-cropping strategy. We subsequently apply the standard ToTensor transformation to normalize pixel values to the $[0, 1]$ range and convert the data into the PyTorch Tensor format for network processing.

4.1. Comparative Results

4.1.1. Qualitative Results

We perform a comprehensive visual comparison between DST-Net and prevailing State-of-the-Art (SOTA) methods to evaluate the perceptual quality of different algorithms in complex real-world scenarios. We select three representative image pairs from the LOL, LSRW-NIKON, and LSRW-HUAWEI benchmarks for demonstration, as



Figure 4: Qualitative comparison of DST-Net with other state-of-the-art algorithms on the LSRW-H dataset.

illustrated in Fig. 3, Fig. 4, 5 and Fig. 6, respectively. From a holistic visual perspective, DST-Net exhibits superior enhancement performance across diverse scenarios characterized by extreme low illumination, color shifts, and intricate textures. The resulting images achieve an optimal balance among brightness restoration, color naturalness, and detail clarity.

Performance on LOL Dataset: Figure 3 illustrates the performance of various methods on the LOL dataset. Most existing algorithms struggle with extreme luminance degradation. Enhancement results from EFINet, LIME, SCI, UTVNet, and Zero-DCE generally exhibit underexposure, where images remain under-illuminated and shadow details are indistinguishable. While EnlightenGAN and NoiSER increase brightness, they induce severe feature loss, with NoiSER further suffering from significant chromatic imbalance. Images generated by LoLiEA, URetinex-Net, ZeroIG, and Zero-DCEP deviate substantially from the Ground Truth (GT) due to pronounced color shifts. Although PairLIE achieves better brightness, it still lacks accurate texture restoration. In contrast, DST-Net successfully restores normal brightness while accurately recovering fine bicycle features and avoiding any obvious color bias.

Performance on LSRW-HUAWEI Dataset: We evaluate the generalization capability of all models by performing inference on the LSRW-HUAWEI dataset using weights pre-trained on the LOL dataset. Figure 4 illustrates these cross-dataset results, which pose a severe challenge to model robustness. Both NoiSER and LIME suffer from catastrophic chromatic collapse and distortion. Among the relatively competitive methods, UTVNet remains constrained by insufficient luminance enhancement. Although HVI-CIDNet and PairLIE maintain color balance, they exhibit evident blurring and structural degradation when processing high-frequency details such as leaf textures. In contrast, DST-Net



Figure 5: Qualitative comparison of DST-Net with other state-of-the-art algorithms on the LSRW-H dataset with zoomed-in patches.

accurately restores colors and preserves fine textures by leveraging illumination-independent feature guidance. These results demonstrate the robust generalization performance of our method, confirming its ability to produce superior visual outcomes in diverse real-world scenarios.

Performance on LSRW-H Dataset (Magnified Details): Figure 5 presents a magnified visual comparison of local details on the LSRW-H dataset to further evaluate enhancement fidelity. The results generated by NoiSER, LoLiEA, LIME, EnlightenGAN, SCI, URetinex_Net, Zero-DCEP, and ZeroIG exhibit pronounced chromatic aberrations, manifesting as a severe purple spectral shift across the visual signal. Furthermore, methods including EFINet, ZeroDCE, Zero-DCEP, and SCI suffer from suboptimal signal amplitude recovery, leading to underexposed images with insufficient overall luminance. In contrast, DST-Net, HVI-CIDNet, and PairLIE demonstrate superior low-light enhancement capabilities, effectively suppressing noise to produce spatially smooth visual representations. Our method clearly recovers sharper object contours and more accurate color distribution compared to others.

Performance on LSRW-NIKON Dataset: Figure 6 presents the visual comparisons on the LSRW-NIKON dataset captured by a DSLR camera. The enhancement results of EnlightenGAN, LIME, NoiSER, ZeroIG, and PairLIE remain unsatisfactory due to persistent artifacts or low contrast. LoLiEA and UTVNet generate images with insufficient overall luminance while UTVNet fails to restore accurate colors for artificial light sources. URetinex-Net suffers from severe overexposure across the entire frame due to excessive illumination correction. Zero-DCE and Zero-DCEP exhibit a distinct cool tone and a noticeable blue shift. Among all evaluated methods, EFINet, HVI-CIDNet, and DST-Net most effectively restore original scene textures. Closer inspection reveals that HVI-CIDNet introduces chromatic deviations

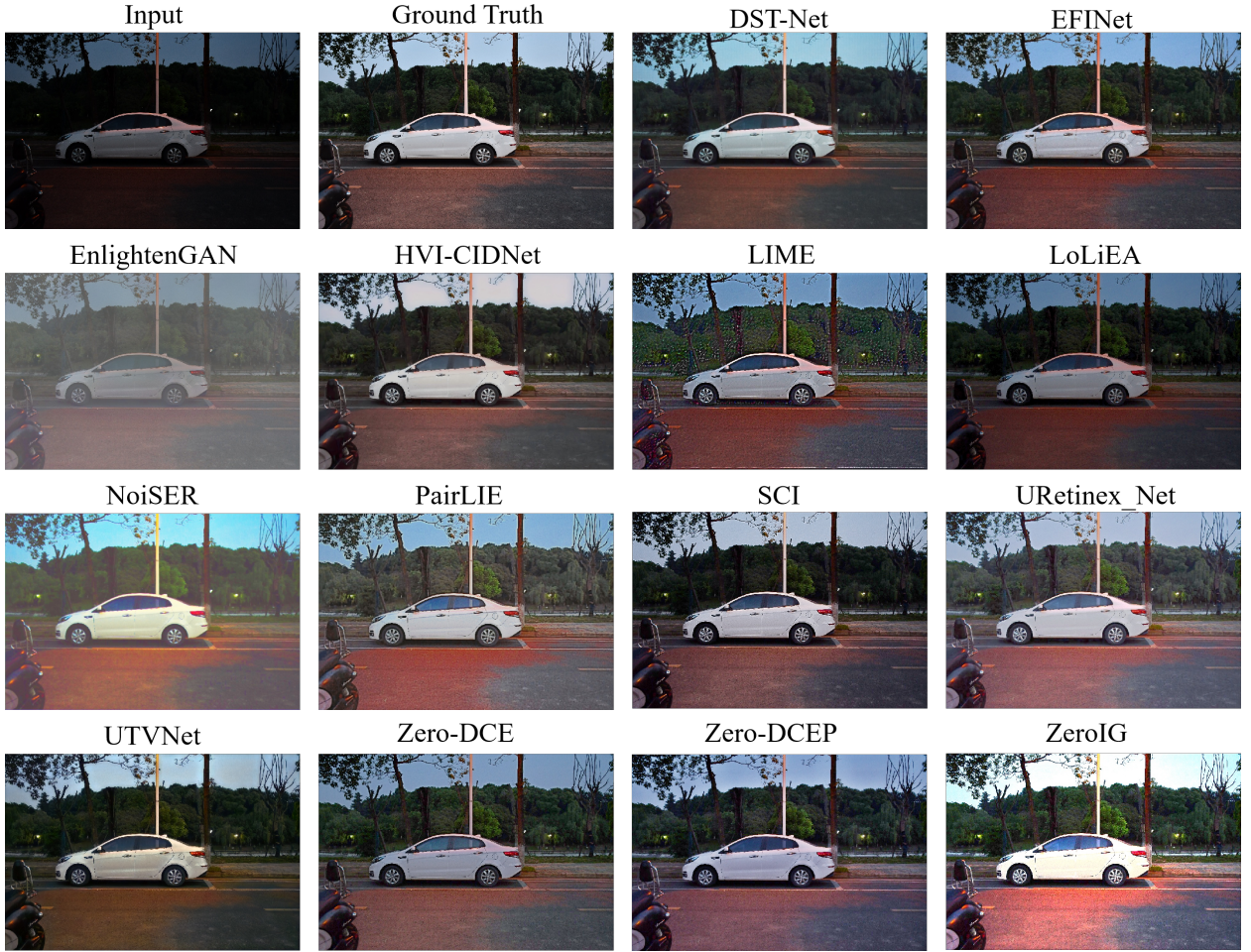


Figure 6: Qualitative comparison of DST-Net with other state-of-the-art algorithms on the LSRW-N dataset.

in sky regions. Collectively, DST-Net achieves optimal performance in exposure control, white balance restoration, and detail reconstruction. Our method provides a visual perception most consistent with real-world scenes.

4.1.2. Quantitative Results

To objectively and quantitatively evaluate enhancement performance, we utilize a multi-dimensional testing framework comprising full-reference and no-reference metrics. The full-reference metrics include Peak Signal-to-Noise Ratio (PSNR), Structural Similarity (SSIM), and Learned Perceptual Image Patch Similarity (LPIPS). The no-reference metrics consist of Lightness Order Error (LOE), Discrete Entropy (DE), and Enhancement Measure (EME). PSNR indicates pixel-level reconstruction quality and luminance fidelity while SSIM evaluates the preservation of geometric structures and textures. The remaining metrics assess perceptual quality, illumination naturalness, and information entropy.

Performance on the LOL Dataset: Table 1 presents the quantitative evaluation results of the compared algorithms on the extreme low-light LOL dataset. DST-Net achieves the highest PSNR value among all evaluated methods. This achievement demonstrates the significant advantages of our approach in luminance restoration, global chromatic fidelity, and noise suppression under extreme low illumination. DST-Net additionally secures the second-highest SSIM score. This performance fully validates the effectiveness of our proposed dual-stream Transformer architecture. By incorporating illumination-independent features from the DoG and LAB spaces as prior guidance, the network prevents

Table 1

Quantitative comparison of DST-Net with other state-of-the-art algorithms on the LOL dataset.

Method	SSIM↑	PSNR↑	LPIPS↓	LOE↓	DE↑	EME↑
HVI-CIDNet [21]	0.9185	25.3487	0.1106	34.0741	2.3893	6.1795
ZeroDceP [16]	0.6750	22.0951	0.2226	12.6747	2.3185	30.6413
ZeroDCE [15]	0.6692	20.8229	0.2054	16.8188	2.1803	30.5752
SCI [33]	0.6386	18.4658	0.1994	1.2873	2.1410	32.0614
RUAS [28]	0.4853	14.2947	0.2396	0.1121	1.4897	34.3492
EnlightenGAN [32]	0.8141	21.0852	0.1788	29.7257	1.6721	3.7087
FmrNet [36]	0.8584	18.0725	0.1438	39.0410	2.5819	5.1740
LIME [27]	0.5651	19.8706	0.3164	88.9189	2.2180	32.9591
FRRNET [37]	0.7259	17.9800	0.2192	6.6306	2.3512	7.4730
UTVNet [30]	0.8773	23.3542	0.1195	17.5475	2.0826	8.4664
ChebyLighter [34]	0.8583	19.8584	0.0871	16.5365	2.4267	6.1861
EFINet [35]	0.7775	18.6969	0.1657	22.1341	1.8055	8.9206
PairLIE [55]	0.8571	24.6975	0.1159	38.6787	2.3218	6.6339
LoLiEA [56]	0.6306	23.9123	0.2365	32.5626	2.2875	10.3545
NoiSER [38]	0.6978	13.7586	0.3635	61.8879	2.6637	4.2352
URetinex_Net [29]	0.8664	19.0972	0.0814	22.9149	2.4423	6.0096
ZeroIG [39]	0.5466	19.8245	0.2825	10.0040	2.8366	31.9599
DST-Net (Ours)	0.9073	25.6400	0.1300	39.5175	2.3851	5.4464

Table 2

Quantitative comparison of DST-Net with other state-of-the-art algorithms on the LSRW-H dataset.

Method	SSIM↑	PSNR↑	LPIPS↓	LOE↓	DE↑	EME↑
HVI-CIDNet [21]	0.6784	20.0579	0.3673	23.6796	2.0622	3.0621
ZeroDceP [16]	0.5586	15.7394	0.3892	19.1252	1.7650	17.0958
ZeroDCE [15]	0.5540	15.5735	0.3526	16.3137	1.6102	17.0669
SCI [33]	0.4906	14.1192	0.3886	3.4174	1.3497	17.5129
RUAS [28]	0.3798	11.4869	0.4568	0.0123	0.9217	17.1161
EnlightenGAN [32]	0.6309	18.2836	0.3330	51.4119	1.5657	1.9064
FmrNet [36]	0.6887	20.3573	0.3396	13.6543	2.2736	2.5441
LIME [27]	0.4002	14.1842	0.5017	109.0293	1.8135	20.5171
FRRNET [37]	0.6568	19.9004	0.3929	23.9182	1.9824	2.6512
UTVNet [30]	0.6585	18.2777	0.2412	19.2575	2.2806	4.1818
ChebyLighter [34]	0.6627	19.6746	0.2963	17.0408	2.1312	3.1945
EFINet [35]	0.5590	13.9895	0.3689	16.4348	1.6485	4.6768
PairLIE [55]	0.6601	19.0896	0.3310	37.4023	1.8716	2.9873
LoLiEA [56]	0.6028	16.8211	0.3766	19.2828	1.8618	6.6287
NoiSER [38]	0.6313	17.4389	0.5122	33.3548	2.0890	1.6669
URetinex_Net [29]	0.6731	20.5522	0.2789	19.0211	2.1614	3.6529
ZeroIG [39]	0.5159	17.7150	0.4046	6.9008	2.0880	17.7718
DST-Net (Ours)	0.7070	20.8486	0.3093	19.5574	2.2160	2.6002

critical feature loss while significantly enhancing image luminance to preserve the physical structure of the original scene.

Performance on the LSRW-HUAWAI Dataset: To further investigate model generalization capabilities, we conduct cross-dataset testing on the LSRW-HUAWAI dataset using weights trained on the LOL dataset without any fine-tuning. Table 2 demonstrates the remarkable generalization performance of DST-Net. Our model achieves the highest scores in the core full-reference PSNR and SSIM metrics. DST-Net additionally outperforms baseline models across the LPIPS, LOE, and DE perceptual and naturalness indicators with the sole exception of the EME metric. This superior

Table 3

Quantitative comparison of DST-Net with other state-of-the-art algorithms on the LSRW-N dataset.

Method	SSIM↑	PSNR↑	LPIPS↓	LOE↓	DE↑	EME↑
HVI-CIDNet [21]	0.5032	17.6521	0.3801	34.5776	1.5881	5.1321
ZeroDceP [16]	0.4228	16.7121	0.3709	34.4376	1.4832	15.7426
ZeroDCE [15]	0.4130	16.0385	0.3613	37.2273	1.2396	15.7546
SCI [33]	0.3723	16.1506	0.3783	17.0591	1.3567	16.7963
RUAS [28]	0.3449	13.5064	0.4063	0.1973	0.9308	16.7991
EnlightenGAN [32]	0.4321	15.6333	0.3838	75.0077	0.9099	2.5021
FmrNet [36]	0.5084	18.1907	0.3362	27.5902	1.7119	3.3538
LIME [27]	0.2865	14.7569	0.4787	102.7659	1.4909	18.7863
FRRNET [37]	0.5010	17.0669	0.4191	48.7073	1.3202	2.6650
UTVNet [30]	0.4678	16.1310	0.3319	23.4239	1.6151	5.7153
ChebyLighter [34]	0.4216	15.3371	0.3742	54.1259	1.6989	4.7313
EFINet [35]	0.4376	15.5073	0.3478	33.3085	1.3715	5.8460
PairLIE [55]	0.4543	17.1800	0.3676	53.1862	1.4388	3.9103
LoLiEA [56]	0.4180	16.0149	0.4088	33.6016	1.4865	12.0068
NoiSER [38]	0.4509	15.9170	0.5532	47.8126	1.4590	2.1554
URetinex_Net [29]	0.4689	17.7877	0.3341	26.9199	1.6173	4.3061
ZeroIG [39]	0.3027	14.5517	0.4630	23.8077	1.6611	16.5508
DST-Net (Ours)	0.5323	17.9031	0.3519	35.1890	1.6687	3.5275

Table 4

DST-Net loss function selection effectiveness ablation learning on the LOL dataset.

Smooth L1	MS-SSIM	TV	EXP	HSV	PSNR↑	SSIM↑
√	√	√	√	×	19.07	0.8154
×	√	√	√	×	16.67	0.7945
√	√	√	×	×	22.14	0.8350
√	×	√	√	×	15.55	0.7264
√	√	×	√	×	19.33	0.8133
√	√	√	√	√	25.47	0.8522

performance strongly indicates that DST-Net accurately controls structural distortion and maintains high visual fidelity when encountering unknown complex degradation scenarios.

Performance on the LSRW-NIKON Dataset: Table 3 reports the quantitative results of the evaluated algorithms on the LSRW-NIKON dataset. Our method maintains top-tier performance on this high-resolution and texture-rich benchmark. DST-Net achieves the highest SSIM score and the second-highest PSNR value. This superior SSIM performance directly reflects the dominance of our network in fine texture reconstruction and edge preservation. We attribute this success primarily to our proposed Multi-Scale Spatial Fusion Block (MSFB). The integrated Pseudo-3D convolutions and explicit Laplacian and Sobel gradient operators deeply exploit spatial correlations across channels. This architectural design maximizes the restoration of high-frequency boundary information under complex low-light conditions.

4.2. Ablation Study

Effectiveness of the Composite Loss Function: We conduct comprehensive ablation experiments on the LOL dataset to validate the objective function design and hyperparameter selection of DST-Net. Table 4 details the quantitative evaluation results for different loss function configurations. The model employing a composite loss formulation including Smooth L1, MS-SSIM, TV, EXP, and HSV components achieves optimal overall performance. DST-Net consistently maintains superior SSIM scores regardless of the specific ablated loss terms. This consistency strongly demonstrates the architectural efficiency in preserving geometric structures and fine textures. The composite loss formulation further drives the model toward a globally optimal solution atop this baseline structural stability.

Table 5

DST-Net performs loss function weight parameter selection ablation learning on the LOL dataset.

w_1	PSNR↑	SSIM↑	w_2	PSNR↑	SSIM↑	w_3	PSNR↑	SSIM↑
$w_1 = 0.5$	23.66	0.9039	$w_2 = 0.1$	18.48	0.8059	$w_3 = 0.1$	22.84	0.9069
$w_1 = 1$	24.75	0.9166	$w_2 = 0.5$	14.95	0.7523	$w_3 = 0.5$	20.54	0.8899
$w_1 = 2$	25.83	0.8886	$w_2 = 1$	23.69	0.8611	$w_3 = 1$	23.58	0.8862
$w_1 = 10$	21.77	0.9114	$w_2 = 1.5$	22.52	0.8587	$w_3 = 2$	23.76	0.8605
$w_1 = 15$	14.51	0.8356	$w_2 = 2$	22.56	0.8521	$w_3 = 5$	20.05	0.8123
			$w_2 = 5$	20.49	0.8230	$w_3 = 15$	18.46	0.7649

Table 6

DST-Net performs feature map validity ablation learning on the LOL dataset.

Color	Structure	Feature	PSNR↑	SSIM↑
×	✓	✓	25.36	0.8836
✓	×	✓	23.68	0.8970
✓	✓	×	22.98	0.8710
✓	✓	✓	25.64	0.9073

Impact of Hyperparameter Weights: To investigate loss weight perturbations on final imaging quality and identify optimal hyperparameters, we perform an ablation study on the MS-SSIM, EXP, and TV loss weights. Table 5 details these quantitative results. **Impact of MS-SSIM Loss Weight (w_1):** We test w_1 values of 0.5, 1, 2, 10, and 15. The SSIM metric peaks at 0.9166 when w_1 equals 1 while the PSNR metric achieves a maximum of 25.83 dB when w_1 equals 2. We select w_1 equal to 1 as the default configuration to maximize the preservation of inherent structural information. The model achieves optimal structural similarity at this weight with negligible PSNR degradation. This setting strikes an optimal balance between pixel and structural fidelity. **Impact of EXP Loss Weight (w_2):** We evaluate the exposure control loss weight w_2 using candidate values of 0.1, 0.5, 1, 1.5, 2, and 5. Both PSNR and SSIM metrics converge and reach maximum values simultaneously when w_2 equals 1. This outcome indicates a positive synergistic effect between appropriate exposure constraints and structural loss. **Impact of TV Loss Weight (w_3):** We evaluate the smoothing loss weight w_3 across candidate values of 0.1, 0.5, 1, 2, 5, and 15. The SSIM metric achieves its maximum value of 0.9069 when w_3 equals 0.1 and consistently declines as the weight increases. Increasing w_3 generates progressively smoother images while excessive smoothing alters underlying structural information to cause this continuous structural degradation. The PSNR metric exhibits a fluctuating trend and peaks at 23.76 when w_3 equals 2 before dropping significantly at larger values.

Effectiveness of Illumination-Independent Feature Maps: We conduct an ablation study on the feature maps to verify the effectiveness and individual contributions of the illumination-independent features within the dual-stream architecture. To maintain structural integrity and parameter consistency, we isolate specific features by filling the corresponding tensor with a minute constant of 10^{-6} rather than deleting the channel. Table 6 details the quantitative results for models lacking color, structural, and textural features. Both PSNR and SSIM metrics exhibit varying degrees of degradation regardless of the disconnected prior feature guidance. This consistent degradation proves that each feature map plays an indispensable role in the low-light restoration task.

5. Conclusion

This paper proposes a Dual-Stream Transformer Network (DST-Net) guided by illumination-independent features and multi-scale spatial fusion convolutions to address image luminance degradation and critical feature loss in low-light environments. Existing methods often struggle to balance color fidelity and texture preservation. DST-Net addresses this deficiency by extracting illumination-independent DoG structural, LAB chromatic, and VGG-16 textural features as priors. The network utilizes a dual-stream interaction architecture and a cross-modal attention mechanism to continuously correct and guide the iterative curve enhancement process. We further design a Multi-Scale Spatial Fusion Block (MSFB) employing pseudo-3D convolutions and explicit 3D gradient operators to deeply exploit spatial correlations across channels and effectively strengthen image edges and fine structures. Extensive comparative

evaluations and ablation studies demonstrate the superior performance of DST-Net. The proposed method achieves a PSNR of 25.64 dB on the LOL dataset while exhibiting robust cross-scenario generalization on the LSRW benchmarks. Future work will optimize algorithmic computational efficiency to facilitate real-time deployment on edge devices and explore application potential in complex scenarios including low-light video sequence enhancement.

Acknowledgments

This work was supported in part by the National Key Research and Development Program of China under Grant 2025YFB2606504.

During the preparation of this manuscript, the author used Google Gemini (Version 3.0 Pro) for the purposes of improving sentence flow and academic tone. The author has reviewed and edited the output and takes full responsibility for the content of this publication.

CRedit authorship contribution statement

Yicui Shi: Conceptualization, Methodology, Visualization, Writing - original draft, Writing - review & editing, Resources, Validation. **Yuhan Chen:** Data curation, Investigation, Writing - review & editing. **Xiangfei Huang:** Validation, Visualization, Resources. **Guofa Li:** Conceptualization, Investigation, Writing - review & editing, Methodology. **Wenxuan Yu:** Validation, Investigation. **Ying Fang:** Validation, Investigation.

Declaration of Competing Interest

The authors declare that they have no known competing financial interests or personal relationships that could have appeared to influence the work reported in this paper.

Data availability

The authors do not have permission to share data.

References

- [1] Q. Zhao, G. Li, B. He, et al., Deep learning for low-light vision: A comprehensive survey, *IEEE Transactions on Neural Networks and Learning Systems* (2025).
- [2] Y. Li, P. Zhou, G. Zhou, et al., A comprehensive survey of visible and infrared imaging in complex environments: Principle, degradation and enhancement, *Information Fusion* 119 (2025) 103036.
- [3] L. Sun, Y. Bao, J. Zhai, et al., Low-light image enhancement using event-based illumination estimation, in: *Proceedings of the IEEE/CVF International Conference on Computer Vision*, 2025, pp. 6667–6677.
- [4] D. Ding, F. Shi, Y. Li, Low-illumination color imaging: Progress and challenges, *Optics & Laser Technology* 184 (2025) 112553.
- [5] Y. M. Alsakar, N. A. Sakr, S. El-Sappagh, et al., Underwater image restoration and enhancement: a comprehensive review of recent trends, challenges, and applications, *The Visual Computer* 41 (6) (2025) 3735–3783.
- [6] V. Jain, Z. Wu, Q. Zou, et al., Ntire 2025 challenge on video quality enhancement for video conferencing: Datasets, methods and results, in: *Proceedings of the Computer Vision and Pattern Recognition Conference*, 2025, pp. 1184–1194.
- [7] P. Singh, A. K. Bhandari, A review on computational low-light image enhancement models: Challenges, benchmarks, and perspectives, *Archives of Computational Methods in Engineering* 32 (5) (2025) 2853–2885.
- [8] Z. He, W. Ran, S. Liu, et al., Low-light image enhancement with multi-scale attention and frequency-domain optimization, *IEEE Transactions on Circuits and Systems for Video Technology* 34 (4) (2023) 2861–2875.
- [9] S. Zheng, Y. Ma, J. Pan, et al., Low-light image and video enhancement: A comprehensive survey and beyond, *arXiv preprint arXiv:2212.10772* (2022).
- [10] Y. Wen, P. Xu, Z. Li, et al., An illumination-guided dual attention vision transformer for low-light image enhancement, *Pattern Recognition* 158 (2025) 111033.
- [11] X. Pei, Y. Huang, W. Su, et al., Fftformer: A spatial-frequency noise aware cnn-transformer for low light image enhancement, *Knowledge-Based Systems* 314 (2025) 113055.
- [12] A. Brateanu, R. Balmez, A. Avram, et al., Lyt-net: Lightweight yuv transformer-based network for low-light image enhancement, *IEEE Signal Processing Letters* (2025).
- [13] J. Guo, J. Ma, Á. F. García-Fernández, et al., A survey on image enhancement for low-light images, *Heliyon* 9 (4) (2023).
- [14] Y. Song, H. Ma, B. Yang, et al., Troublemaker learning for low-light image enhancement, in: *Proceedings of the 2025 International Conference on Multimedia Retrieval*, 2025, pp. 1172–1181.
- [15] C. Guo, C. Li, J. Guo, C. C. Loy, J. Hou, S. Kwong, D. Tao, Zero-reference deep curve estimation for low-light image enhancement, in: *Proceedings of the IEEE/CVF conference on computer vision and pattern recognition*, 2020, pp. 1780–1789.
- [16] C. Li, C. Guo, C. C. Loy, Learning to enhance low-light image via zero-reference deep curve estimation, *IEEE Transactions on Pattern Analysis and Machine Intelligence* 44 (8) (2021) 4225–4238.
- [17] R. Xu, Y. Niu, Y. Li, et al., Urwkv: Unified rwkv model with multi-state perspective for low-light image restoration, in: *Proceedings of the IEEE/CVF Conference on Computer Vision and Pattern Recognition*, 2025, pp. 21267–21276.
- [18] Y. Lin, X. Xu, J. Wu, et al., Geometric-aware low-light image and video enhancement via depth guidance, *IEEE Transactions on Image Processing* (2025).
- [19] Y. Qi, Z. Yang, W. Sun, et al., A comprehensive overview of image enhancement techniques, *Archives of Computational Methods in Engineering* 29 (1) (2022) 583–607.
- [20] L. Xu, C. Hu, Y. Hu, et al., Upt-flow: Multi-scale transformer-guided normalizing flow for low-light image enhancement, *Pattern Recognition* 158 (2025) 111076.
- [21] Q. Yan, Y. Feng, C. Zhang, et al., Hvi: A new color space for low-light image enhancement, in: *Proceedings of the computer vision and pattern recognition conference*, 2025, pp. 5678–5687.
- [22] Y. Sun, W. Wang, Role of image feature enhancement in intelligent fault diagnosis for mechanical equipment: A review, *Engineering Failure Analysis* 156 (2024) 107815.
- [23] S. M. Pizer, E. P. Amburn, J. D. Austin, R. Cromartie, A. Geselowitz, T. Greer, B. ter Haar Romeny, J. B. Zimmerman, K. Zuiderveld, Adaptive histogram equalization and its variations, *Computer vision, graphics, and image processing* 39 (3) (1987) 355–368.
- [24] S.-C. Huang, F.-C. Cheng, Y.-S. Chiu, Efficient contrast enhancement using adaptive gamma correction with weighting distribution, *IEEE transactions on image processing* 22 (3) (2012) 1032–1041.
- [25] E. H. Land, The retinex theory of color vision, *Scientific american* 237 (6) (1977) 108–128.
- [26] D. J. Jobson, Z.-u. Rahman, G. A. Woodell, A multiscale retinex for bridging the gap between color images and the human observation of scenes, *IEEE Transactions on Image processing* 6 (7) (1997) 965–976.
- [27] X. Guo, Y. Li, H. Ling, Lime: Low-light image enhancement via illumination map estimation, *IEEE Transactions on image processing* 26 (2) (2016) 982–993.
- [28] R. Liu, L. Ma, J. Zhang, Y. Xin, Z. Luo, Retinex-inspired unrolling with cooperative prior architecture search for low-light image enhancement, in: *Proceedings of the IEEE/CVF conference on computer vision and pattern recognition*, 2021, pp. 10561–10570.
- [29] W. Wu, J. Wang, M. Gong, Y. Yang, et al., Uretinex-net: Retinex-based deep unfolding network for low-light image enhancement, in: *Proceedings of the IEEE/CVF conference on computer vision and pattern recognition*, 2022, pp. 5901–5910.
- [30] C. Zheng, D. Shi, W. Shi, Adaptive unfolding total variation network for low-light image enhancement, in: *Proceedings of the IEEE/CVF International Conference on Computer Vision*, 2021, pp. 4439–4448.
- [31] Z. Fu, Y. T. Yang, X. Tu, et al., Learning a simple low-light image enhancer from paired low-light instances, in: *Proceedings of the IEEE/CVF Conference on Computer Vision and Pattern Recognition*, 2023, pp. 22252–22261.
- [32] Y. Jiang, X. Gong, D. Liu, Y. Cheng, C. Fang, X. Shen, J. Yang, P. Zhou, Z. Wang, Enlightengan: Deep light enhancement without paired supervision, *IEEE transactions on image processing* 30 (2021) 2340–2349.

- [33] L. Ma, T. Ma, R. Liu, X. Fan, Z. Luo, Toward fast, flexible, and robust low-light image enhancement, in: Proceedings of the IEEE/CVF conference on computer vision and pattern recognition, 2022, pp. 5637–5646.
- [34] J. Pan, D. Zhai, Y. Bai, et al., Cheblyghter: Optimal curve estimation for low-light image enhancement, in: Proceedings of the 30th ACM International Conference on Multimedia, 2022, pp. 1358–1366.
- [35] C. Liu, F. Wu, X. Wang, Efinet: Restoration for low-light images via enhancement-fusion iterative network, *IEEE Transactions on Circuits and Systems for Video Technology* 32 (12) (2022) 8486–8499.
- [36] Y. Chen, X. Wang, Z. Li, et al., Fmr-net: a fast multi-scale residual network for low-light image enhancement, *Multimedia Systems* 30 (2) (2024) 73.
- [37] Y. Chen, X. Wang, Z. Li, et al., Frr-net: a fast reparameterized residual network for low-light image enhancement, *Signal, Image and Video Processing* 18 (5) (2024) 4925–4934.
- [38] Z. Zhang, S. Zhao, X. Jin, et al., Noise self-regression: A new learning paradigm to enhance low-light images without task-related data, *IEEE Transactions on Pattern Analysis and Machine Intelligence* 47 (2) (2024) 1073–1088.
- [39] Y. Shi, D. Liu, L. Zhang, et al., Zero-ig: Zero-shot illumination-guided joint denoising and adaptive enhancement for low-light images, in: Proceedings of the IEEE/CVF conference on computer vision and pattern recognition, 2024, pp. 3015–3024.
- [40] Y. Chen, Y. Shi, G. Li, et al., A lightweight real-time low-light enhancement network for embedded automotive vision systems, *arXiv preprint arXiv:2512.02965* (2025).
- [41] J. Li, F. Fang, K. Mei, G. Zhang, Multi-scale residual network for image super-resolution, in: Proceedings of the European conference on computer vision (ECCV), 2018, pp. 517–532.
- [42] S. W. Zamir, A. Arora, S. Khan, M. Hayat, F. S. Khan, M.-H. Yang, L. Shao, Learning enriched features for real image restoration and enhancement, in: Proceedings of the European Conference on Computer Vision (ECCV), 2020, pp. 492–511.
- [43] S.-J. Cho, S.-W. Ji, J.-P. Hong, et al., Rethinking coarse-to-fine approach in single image deblurring, in: Proceedings of the IEEE/CVF International Conference on Computer Vision, 2021, pp. 4641–4650.
- [44] Y. Dai, F. Gieseke, J. Oeppen, et al., Attentional feature fusion, in: Proceedings of the IEEE/CVF Winter Conference on Applications of Computer Vision, 2021, pp. 3560–3569.
- [45] J. Hu, L. Shen, G. Sun, Squeeze-and-excitation networks, in: Proceedings of the IEEE conference on computer vision and pattern recognition, 2018, pp. 7132–7141.
- [46] S. Woo, J. Park, J.-Y. Lee, I. S. Kweon, Cbam: Convolutional block attention module, in: Proceedings of the European conference on computer vision (ECCV), 2018, pp. 3–19.
- [47] X. Qin, Z. Wang, Y. Bai, et al., Ffa-net: Feature fusion attention network for single image dehazing, in: Proceedings of the AAAI Conference on Artificial Intelligence, 2020, pp. 11908–11915.
- [48] C. Wei, W. Wang, W. Yang, J. Liu, Deep retinex decomposition for low-light enhancement, *arXiv preprint arXiv:1808.04560* (2018).
- [49] Y. Zhang, X. Guo, J. Ma, W. Liu, J. Zhang, Beyond brightening low-light images, *International Journal of Computer Vision* 129 (4) (2021) 1013–1037.
- [50] L. Ma, T. Ma, R. Liu, et al., Structure-preserving low-light image enhancement, in: Proceedings of the European Conference on Computer Vision (ECCV), 2022, pp. 245–261.
- [51] X. Xu, R. Wang, C.-W. Fu, et al., Snr-aware low-light image enhancement, in: Proceedings of the IEEE/CVF Conference on Computer Vision and Pattern Recognition, 2022, pp. 17714–17724.
- [52] Z. Cui, K. Li, L. Gu, et al., You only need 90k parameters to adapt light: a light weight transformer for image enhancement and exposure correction, *arXiv preprint arXiv:2205.14871* (2022).
- [53] Y. Cai, H. Bian, J. Lin, et al., Retinexformer: One-stage retinex-based transformer for low-light image enhancement, in: Proceedings of the IEEE/CVF international conference on computer vision, 2023, pp. 12504–12513.
- [54] J. Hai, et al., R2rnet: Low-light image enhancement via real-low to real-normal network, *Journal of Visual Communication and Image Representation* 90 (2023) 103712.
- [55] W. Yang, S. Wang, Y. Fang, et al., From fidelity to perceptual quality: A semi-supervised approach for low-light image enhancement, in: Proceedings of the IEEE/CVF conference on computer vision and pattern recognition, 2020, pp. 3063–3072.
- [56] E. Perez-Zarate, O. Ramos-Soto, E. Rodríguez-Esparza, et al., Loli-ia: low-light image enhancement algorithm, in: *Applications of Machine Learning* 2023, Vol. 12675, SPIE, 2023, pp. 248–263.